sustainability

MDPI

Article

Experimental Study on the Use of Iron Tailings-Based Multicomponent Solid Waste as SCMs

Yannian Zhang [1,2], Houqi Sun [2], Xiaowei Gu [3], Wenjie Zhang [2] and Bonan Liu [2,*]

[1] School of Civil Engineering, Jilin University of Architecture and Technology, Changchun 130114, China; zyntiger@163.com
[2] College of Civil Engineering, Shenyang Jianzhu University, Shenyang 110168, China; shq3465528710@outlook.com (H.S.); zwj60141841@outlook.com (W.Z.)
[3] School of Resources and Civil Engineering, Northeastern University, Shenyang 110819, China; guxiaowei@mail.neu.edu.cn
* Correspondence: m18342831904@outlook.com

Abstract: A considerable amount of carbon dioxide is released during the preparation of traditional Portland cement, which is not in conformity with the sustainable road. Developing supplementary cementitious material (SCMs) and reducing cement consumption are safe ways to solve this problem. Iron tailings (IOTs), a type of mining waste from the beneficiation process of iron ore concentrate, can be used as SCMs in concrete. In order to tackle the problem of low compressive performance of IOTs as SCMs in concrete, this study develops a multi-SCMs system based on IOTs. Mechanical properties and microstructure of samples with different activator contents and ratios were analyzed by compressive strength, differential thermal–thermal gravimetric analysis (DTA-TG), and scanning electron microscopy (SEM). The results show that the compressive strength of the composite gel blocks in different gel systems changed as follows: ternary SCMs system > binary SCMs system > unary SCMs system. The ternary SCMs system (IOTs: Steel slag(SS):Phosphorus slag(PS) = 1:2:2) without activator was added so that it resulted in the highest compressive strength in multi-SCMs system. With the increase in the content of activators, the compressive strength with ternary SCMs system shows a decreasing trend. It is well known from DTA-TG, as well as SEM, that NaOH and Na_2SiO_3 have an inhibitory effect on the secondary hydration reaction and inhibit the formation of C-S-H gel.

Keywords: iron tailings; steel slag; phosphorus slag; mortar specimen; compressive strength; microscopic analysis

Citation: Zhang, Y.; Sun, H.; Gu, X.; Zhang, W.; Liu, B. Experimental Study on the Use of Iron Tailings-Based Multicomponent Solid Waste as SCMs. *Sustainability* **2022**, *14*, 5124. https://doi.org/10.3390/su14095124

Academic Editors: Gabriela Ionescu, Ioannis Katsoyiannis, Marco Ragazzi, Elena Magaril, Elena Rada, Paolo Viotti, Hussain H. Al-Kayiem, Marco Schiavon and Natalia Sliusar

Received: 24 March 2022
Accepted: 18 April 2022
Published: 24 April 2022

1. Introduction

Due to the rapid development of the national economy. The increasing demand for natural energy and resources has produced a large amount of solid waste in China. To reduce the impact on the environment and achieve sustainability, solid waste should be used again. Most solid waste is mainly used in the concrete industry [1]. These waste materials can be used to partially replace cement or aggregate in concrete [2–5]. The most commonly used solid wastes in modern concrete are blast furnace slag and fly ash [6–8] due to the high activity of blast furnace slag that can be used to replace more cement. However, the high content of blast furnace slag leads to a large dry shrinkage in the later stage [9]. Moreover, the demand for blast furnace slag exceeds its supply in China. In order to ensure the sustainable development of the concrete industry, other industrial wastes must be used in concrete.

It is known that China has a large capacity for IOTs production. The data shows that the comprehensive utilization ratio of IOTs in China is only 10%, which is far from 60% of developed countries [10]. Large quantities of IOTs are piling up, occupying land, and polluting air and water. Song et al. [1] studied the influence of IOTs as SCMs on the mechanical properties and microstructure of concrete. It is proved that IOTs can be used as

SCMs instead of cement. Liu [11] revealed the fracture and reconstruction of Si–O–Si in IOTs, revealing the feasibility of IOTs powder as concrete admixture from a microscopic perspective. Yun Hong et al. [12] reported that mechanochemically activated IOTs have volcanic ash properties and can be used as SCMs in concrete. Ma et al. [13] noted that the density and compressive strength of concrete can be fully improved by using 40–60% silica instead of adding IOTs in autoclaved aerated concrete, which meets the requirements of national standards B05 and A2.5. In China, the generation of SS is huge, but the total utilization rate is low. The data shows that the comprehensive utilization ratio of SS in China is only 20%, which is far from 90% of developed countries. It was estimated that over one million tons of SS is impounded in China [14]. The main chemical composition of SS is similar to cement clinker, which is a potentially active cementitious material. Han et al. [15] believe that SS could improve workability, decrease its hydration heat, fill the internal micropores, and enhance its interfacial transition zone (ITZ). Yang et al. [16] indicate that SS powders added to magnesium potassium phosphate cement (MKPC) paste can significantly improve the samples' early mechanical strength. PS is a by-product generated by yellow phosphorus production, and many PS are discharged in China [17]. Large quantities of PS are piling up, occupying land, and polluting air and water. PS and blast furnace slag have similar chemical composition and also have certain activity. Research has shown that the wear-resisting strength of concretes can be enhanced by fly ash with PS [18]. Therefore, using IOTs, PS, and SS to replace part of cement can effectively consume these three kinds of bulk solid wastes.

Research has shown that [19] IOTs alone as SCMs has an adverse effect on compressive performance. Other studies have shown [20–22] IOTs, PS, and SS can be stimulated to be active under alkaline conditions, respectively. The coexcitation of the ternary SCMs system of IOTs, SS, and PS under alkaline environment has not been studied. SS and PS as a high-calcium type solid waste has a similar chemical composition to cement and can undergo hydration reactions to produce C-S-H. In addition, IOTs can play a filling role. Theoretically, the three have some synergistic effects and can be used together to achieve the effect of consuming a large amount of solid waste.

In this paper, we used NaOH and Na_2SiO_3 to provide an alkaline environment and investigated the mechanical properties and the formation and evolution of hydration products of a multi-SCMs system by compressive strength test, DTA-TG, and SEM. A theoretical basis is provided for an in-depth study of multi-SCMs based on IOTs.

2. Experiments

2.1. Raw Materials

In this experiment, the cement was produced by Benxi Shan shui Gong yuan Cement Co., Ltd. (Shenyang, China) the performance of which conforms to the requirements of GB175-2007 [23] "General Silicate Cement". The sand used in the study was ISO standard sand. The cumulative sieve margin of ISO sand through 2 mm, 1.6 mm, 1.0 mm, 0.5 mm, 0.16 mm, and 0.08 mm square sieve is 0%, 7%, 33%, 67%, 87%, and 99%, respectively. The water absorption of ISO sand is less than 0.2%. NaOH and Na_2SiO_3 are taken from Xilong Chemical Company (Shantou, China) with a purity of 99% and the modulus of Na_2SiO_3 is 1. The IOTs are taken from Waitoushan, Benxi, Liaoning Province, China. SS is taken from Shanghai Baowu Group. PS is taken from Yunnan Kunming Haifu Trading Co., Ltd. (Kunming, China). SS meet the experimental requirements and is no longer ground. The PS and IOTs were ground in 100 t/h horizontal ball mill for 1.5 h. The specific surface area of IOTs, PS, and SS are 1290 cm^2/g, 594.5 cm^2/g, and 1020 cm^2/g. All the SCMs selected are in accordance with GB/T51003-2014 [24]. The chemical composition of each substance is shown in Table 1. The particle size distribution of IOTs, SS, and PS are shown in Figure 1. The morphology of raw materials is shown in Figure 2.

Table 1. Chemical composition of raw materials%.

Composition	CaO	SiO_2	Al_2O_3	Fe_2O_3	MgO	SO_3	LOI	Others
Cement	56.1	23.6	6.89	2.69	3.96	2.69	3.20	4.07
IOT	7.77	62.26	4.78	14.37	6.33	0.48	2.39	4.01
SS	42.65	15.20	2.53	27.54	6.05	0.12	2.18	5.46
PS	47.45	39.08	3.94	1.14	2.90	1.22	2.70	4.27

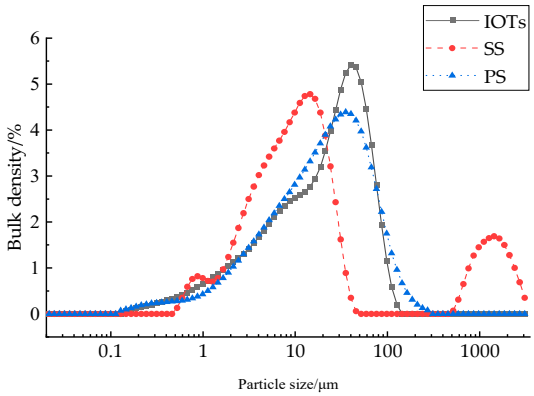

Figure 1. Particle size distribution of IOTs, PS and SS.

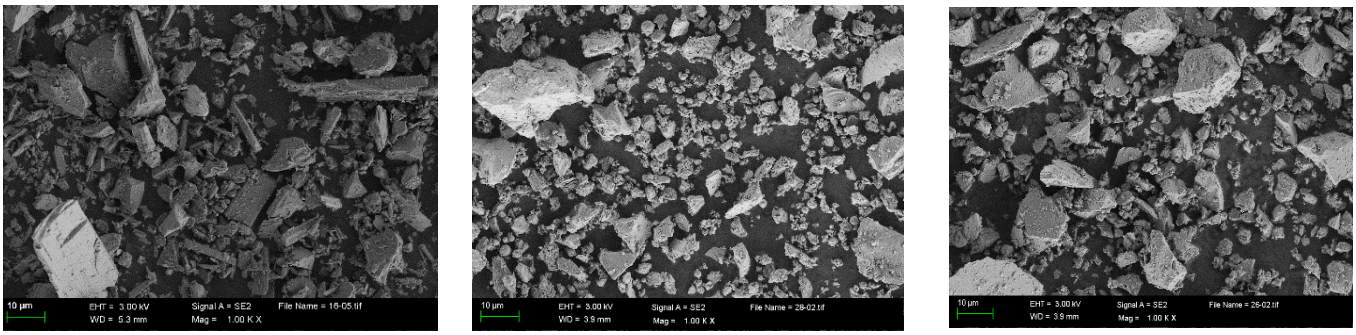

(**a**) (**b**) (**c**)

Figure 2. SEM image of (**a**) IOTs; (**b**) SS; (**c**) PS.

From Figure 1, it can be seen that there is a particle size of about 1000 um in the SS. However, comparing the SEM images in Figure 2, it is found that the particle size of SS is similar to that of IOTs and PS, and even somewhat smaller than that of IOTs and PS. This is because the SEM images are taken at different points, and the particle size of about 1000 um is not a large proportion of the SS. Therefore, the particle size in the SEM map does not correspond exactly to the particle size distribution map.

2.2. Sample Preparation

Cement paste: The required raw materials were poured into a JJ-5 planetary mixer to produce paste as per China standard GB/T17671-1999 [25]. We prepared 20 mm × 20 mm × 20 mm test blocks and placed them in a maintenance room with (20 ± 1) °C and relative humidity greater than 95%. After 24 h, the mold was removed and cured in water for 7 d and 28 d [26]. The replacement levels of SCMs were 30% by mass, and water-to-binder (*w/b*) ratios of 0.5 were used in this study [26]. Microscopic experiments were performed according to the ratios in Table 2.

Table 2. Composition of the paste analyzed.

Serial Number	Cement/g	Water/g	Sand/g	IOT/g	SS/g	PS/g	Activator
PB5	315	135	0	27	54	54	0
PC2	315	135	0	27	54	54	0.6% NaOH
PD2	315	135	0	27	54	54	0.6% Na_2SiO_3

Cement mortar: The required raw materials were poured into a JJ-5 planetary mixer to produce mortars as per China standard GB/T17671-1999 [25]. Preparation of 40 mm × 40 mm × 160 mm prismatic specimens (six prismatic specimens need to be prepared for each group of mortar, and three prismatic specimens need to be tested at each age) according to GB/T17671-1999 [25] and placed in a curing room with a relative humidity of more than 95% at (20 ± 1) °C. The mold was removed after 24 h, and the strength was measured after curing in water for 7 d and 28 d [26]. The replacement levels of SCMs were 30% by mass, and water-to-binder (*w/b*) ratios of 0.5 were used in this study [26]. The specific ratio is shown in Tables 3–5.

Table 3. Composition of the different admixture systems.

Serial Number	Cement/g	Water/g	Sand/g	IOT/g	SS/g	PS/g
BZ	450	225	1350	0	0	0
T0	315	225	1350	135	0	0
T1	315	225	1350	67.5	67.5	0
T2	315	225	1350	67.5	0	67.5
T3	315	225	1350	0	67.5	67.5
T4	315	225	1350	45	45	45

Table 4. Composition of the proportion of ternary SCMs system.

Serial Number	Cement/g	Water/g	Sand/g	IOT/g	SS/g	PS/g
BZ	450	225	1350	0	0	0
B1	315	225	1350	67.5	50.6	16.9
B2	315	225	1350	67.5	33.8	33.8
B3	315	225	1350	67.5	16.9	50.6
B4	315	225	1350	45	45	45
B5	315	225	1350	27	54	54

Table 5. Composition of the effect of activator on strength of ternary SCMs system.

Serial Number	Cement/g	Water/g	Sand/g	IOT/g	SS/g	PS/g	Activator/g
C0	315	225	1350	27	54	54	0
C1	315	225	1350	27	54	54	0.54 g NaOH
C2	315	225	1350	27	54	54	0.81 g NaOH
C3	315	225	1350	27	54	54	1.08 g NaOH
C4	315	225	1350	27	54	54	1.35 g NaOH
C5	315	225	1350	27	54	54	1.62 g NaOH
D1	315	225	1350	27	54	54	0.54 g Na_2SiO_3
D2	315	225	1350	27	54	54	0.81 g Na_2SiO_3
D3	315	225	1350	27	54	54	1.08 g Na_2SiO_3
D4	315	225	1350	27	54	54	1.35 g Na_2SiO_3
D5	315	225	1350	27	54	54	1.62 g Na_2SiO_3

2.3. Experimental Methods

2.3.1. Strength Test Method

The strength of mortar was tested with a YES-2000B testing machine according to GB/T17671-1999 [25]. Compressive strength R_c takes Newton per square millimeter (MPa) as the unit and is calculated according to the following equation:

$$Rc = Fc/A \quad (1)$$

where F_c is the maximum load at the time of failure, and A is the compressed area.

The compressive strength of mortar at the age of 7 d and 28 d was measured according to the national standard GB/T17671-1999 [25]. One mortar sample was broken into two segments on the flexural testing machine. Then, the two segments were used to measure the compressive strength of mortar. The compressive strength of one sample is the average value of compressive strengths of six segments (three mortars). The activity index of 7 d and 28 d mortar was measured according to the national standard GB/T12957-2005 [26]. The activity index can be calculated according to the following equation:

$$K = R_1/R_2 \times 100\% \quad (2)$$

where R_1 is the compressive strength of the admixture system test sample at 7 d and 28 d. R_2 is the compressive strength of the cement mortar for 7 d and 28 d.

2.3.2. Fluidity Test Method

The fluidity of fresh mortars was tested according to GB/T 2419-2005 [27], which was called the flow table test. Details of the flow table test were as follows. Fresh mortars were cast into a trapeziform metal container above a rounded table, and then vibrated 25 times for 25 s, moving freely without the container until plates of fresh mortars stopped. The diameters of fresh mortar plates were recorded, and the average value was determined for fluidity of fresh mortars.

2.3.3. Microscopic Test

Blended pastes mixed with cement were adopted using the following measurement: DTA-TG, SEM. The paste experimental compositions used in the paste experiments are shown in Table 2.

In this experiment, the hydration products were determined and analyzed by SEM. QUANTA200 scanning electron microscope was used to analyze the hydration products, soaking in absolute ethyl alcohol for more than 24 h and screening out thin sample fragments relatively. The setting temperature of the oven should not exceed 60 °C, so as not to cause carbonization on the surface of the sample. After the surface of the sample fragments was gilded, the samples were placed under different multiples of caning electron microscope to observe their microscopic morphology and mineral structure.

The comprehensive thermal analyzer was used to analyze the endothermic, exothermic and gaseous changes of cement hydration products. Differential thermal thermogravimetric analysis is used to calculate the content of $Ca(OH)_2$ of hydration products according to the thermal peak and weight loss of the DTA-TG curve, and the degree of hydration reaction can be judged quantitatively, soaking in absolute ethyl alcohol for more than 24 h and screening out thin sample fragments relatively and grinding into powder. The testing parameters of the measuring instrument are set as follows: nitrogen is used as the protective gas in the furnace, the temperature of the circulating water of the instrument is controlled at about 25 °C, and the reference sample is $A1_2O_3$. Heating system: initial temperature 20 °C; 10 °C per minute heating rate to furnace temperature of up to 800 °C.

3. Results and Discussion

3.1. Destruction Form

In the process of loading, the damage form of compressive strength is mainly manifested by the vertical compression deformation of the specimen and the transverse tensile deformation. When the specimen is near the ultimate load, vertical cracks appear in the middle and extend to the upper and lower ends and corners, finally forming cracks in the inverted figure of eight. Cracks develop continuously from outside to inside after the ultimate load, mortar debris comes off the surface of the specimen, and the damage form of the specimen after unloading is a quadrangular cone with positive and negative connections.

3.2. Compressive Strength

3.2.1. Different SCMs Systems

Figure 3 shows the influence of different SCMs systems on compressive strength and activity index. As can be seen from Figure 3a, compared with the Bz, the early strength of each group with admixture decreased significantly which the highest activity index for 7 d was only 83%. The reason is that the early activity of the SCMs system is low. The pozzolanic reaction of IOTs, SS, and PS are weak, which only plays a filling role in the early hydration stage [2].

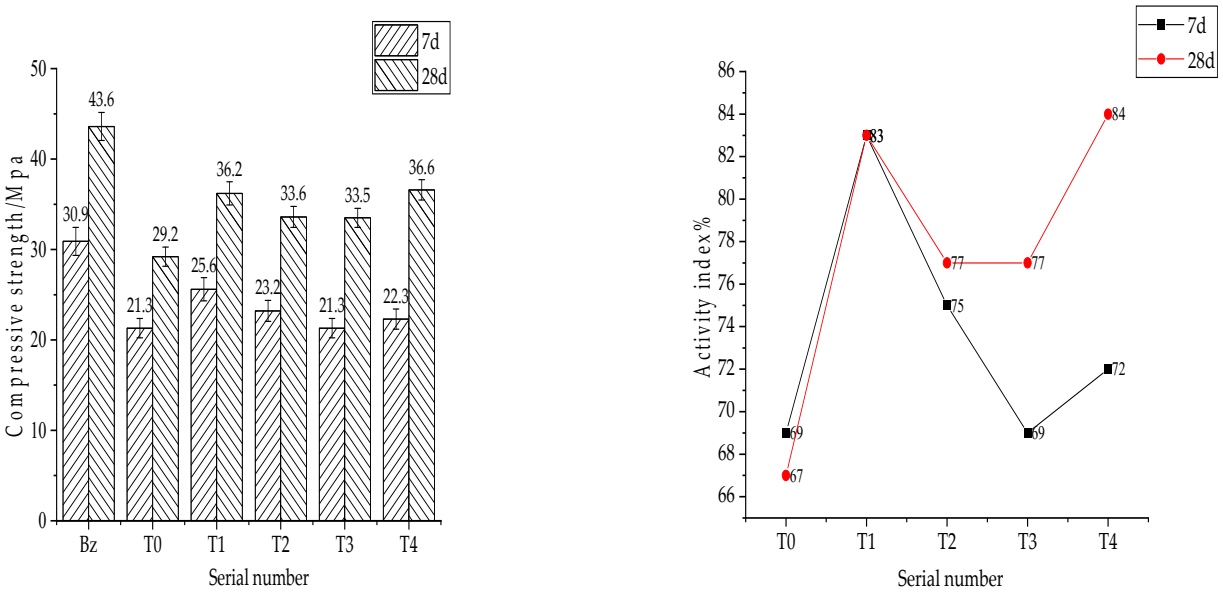

(**a**) compressive sterngth (**b**) activity index

Figure 3. The compressive strength and activity index of the different SCMs systems.

As can be seen from Figure 3a, the compressive strength of T0 is the lowest among all ages. Although IOTs contain more SiO_2 (Table 1), most of them are crystalline phase with low overall activity and basically no pozzolanic activity [1]. Therefore, when IOTs are used as SCMs alone, it mainly plays a filling effect [11]. Using IOTs in combination with SS and PS can obviously improve the negative effect of IOTs on compressive properties. In the binary SCMs system, the strength of T1 is significantly higher than that of T2 because the phosphorus and fluorine contained in the PS reacts with the CH produced by hydration producing fluorohydroxyapatite and calcium phosphate, which cover the surface of cement particles and inhibit the hydration of cement particles [18]. In addition, at the initial stage of hydration, soluble phosphorus can stabilize the hexagonal hydrate of C_3A and prevent it from transforming into cubic hydration products, which result in retarding. So, the strength is not high [28]. Compared with T3 and T4, blindly reducing the content of IOTs or increasing the amount of SS and PS cannot improve the 28d compressive strength. Some

studies [29] have shown that the nucleation and filling of IOTs are essential for the strength of the whole system. Consistent with the results of this paper.

3.2.2. Proportion of Ternary SCMs System

Figure 4 illustrates the influence of ternary SCMs systems with different proportions on compressive strength and activity index. As can be seen in Figure 4a, the addition of the SCMs leads to a lower overall compressive strength compared with Bz, indicating that the activity of the SCMs is lower than that of the cement [30]. Compared with B1, B2, and B3, with the increase in PS and the decrease in SS, the 28d compressive strength gradually decreases. It can be seen from Section 3.2.1 that there are substances in PS that inhibit cement hydration [27]. In addition, SS promotes 28 d hydration [31]. When the content of IOTs in the system is higher, the 28d compressive strength is lower. However, when the content of SS and PS are higher, the 28d compressive strength is higher. Especially the ternary SCMs system (IOTs:SS:PS = 1:2:2), which has the highest compressive strength and activity index in a multi-SCMs system. This is due to the different hydration activity of different SCMs. SS and PS are mainly high-calcium glass phase, which make a great contribution to the pozzolanic effect. Combined with Section 3.2.1, it is known that IOTs are mainly crystalline SiO_2. Without any means of activation, IOTs can be simply considered to be a kind of inert material. Some scholars believe that [9] the role of IOTs is similar to that of limestone, which IOTs not only play a filling role in but also a nucleation role [32]. As the crystal nucleus of hydration products, small IOTs particles reduce the nucleation barrier and accelerate the formation of C-S-H gel in the process of hydration. However, because of its low activity, IOTs should not exceed 5% [33] of cementitious materials, otherwise its nucleation and filling effect cannot counteract its negative effects on hydration.

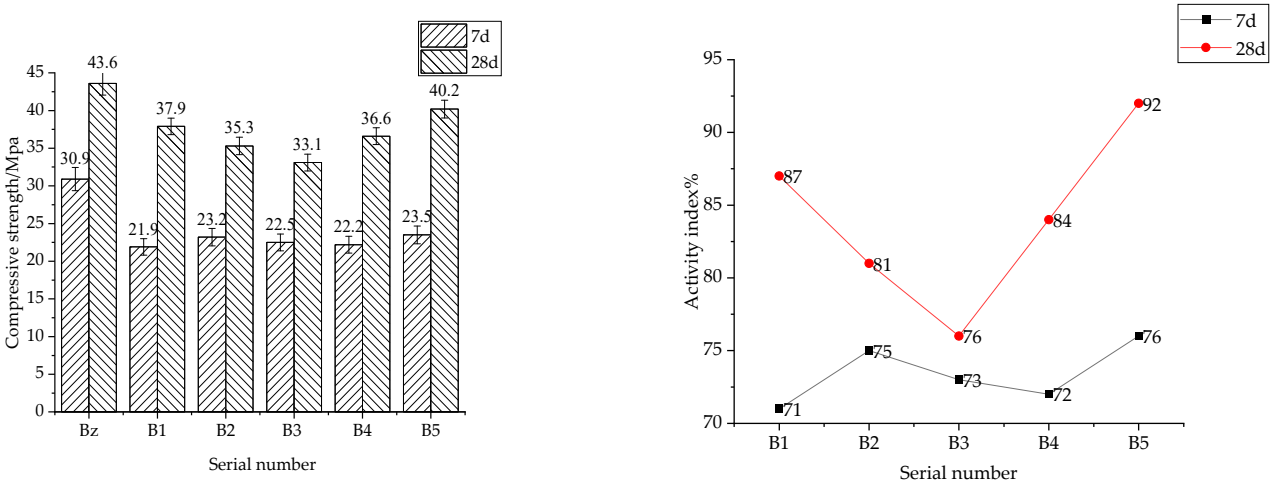

(**a**) compressive sterngth (**b**) activity index

Figure 4. The compressive strength and activity index of the proportion of ternary SCMs system.

Therefore, the action mechanism of the multi-SCMs system can be simply summarized as follows: IOTs accelerate the hydration of cement particles through nucleation effect, which produces more C-S-H gel and CH. CH release OH^- to destroy the glass phase of SS and PS, promoting the dissolution and reaction of active ions and resulting in hydration products such as C-S-H gel to improve strength.

3.2.3. Multiple Regression Analysis

The effects of the composition of IOTs, PS, and SS on the 7 d and 28 d compressive strengths were discussed by multiple regression analysis, and the following equations were obtained:

$$y_7 = 31.010 - 0.069x_1 - 0.071x_2 - 0.105x_3 \quad (3)$$

$$y_{28} = 43.84 - 0.11x_1 - 0.03x_2 - 0.10x_3 \quad (4)$$

In the Equations (3) and (4), y represents the compressive strength (MPa), x_1 represents the content of IOTs (%), x_2 represents the content of SS (%), and x_3 represents the content of PS (%).

The fitted values of compressive strength calculated by the models are compared with the actual measured values, so that the fitting effect of each model can be observed more visually. Figure 5 shows the comparison of the fitted strength with the measured strength for different ratios at each age. The distribution of the points is observed in the figure with the linear function y = x as a reference, and the closer the points are to the straight line indicates that the fitted value is closer to the measured compressive strength. As can be seen from Figure 5, the difference between the fitted and measured values is fewer than 2 MPa for most of the points, except for very few points with large deviations, and even some of the fitted values agree with the measured values, which means that the simulation effect is good.

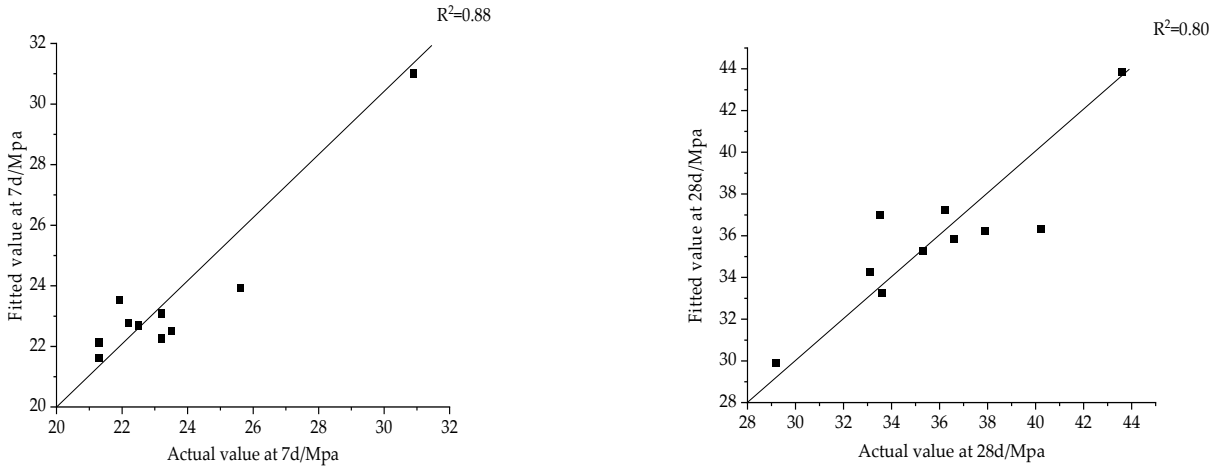

(**a**) at 7 d (**b**) at 28 d

Figure 5. Comparison of fitted with tested compressive strength of ternary SCMs system with different proportions at 7 d and 28 d.

3.2.4. Effect of Activator on Strength of Ternary SCMs System

It can be seen from Figure 6 that the chemical activator NaOH to the ternary SCMs system has an inhibitory effect on the compressive strength and activity index of the whole age. For 7 d compressive strength, the change in NaOH content has little effect on it. At the age of 28 d, as the content of NaOH increased from 0% to 1.2%, the compressive strength decreased 5.9 MPa and the activity index decreased by about 13%.

The addition of NaOH in the whole system provides an alkaline environment for the hydration of IOTs, SS, and PS, but the compressive strength does not increase as expected. The reasons are as follows: (1) The hydration of cement itself produces CH that createsg an alkaline environment. NaOH restrains the hydration of cement itself after adding strong alkalinity, resulting in a decrease in strength [34,35]. (2) The increase in NaOH concentration may lead to the rapid formation of hydration products in the paste. In addition, a large number of these hydration products are attached to the surface of PS, SS, and other particles, which hinders the further hydration of the particles to some extent [36]. (3) The high content of Cstroke S in the system leads to the lack of active SiO_2, which cannot transform calcium silicate hydrate with high alkalinity to calcium silicate hydrate with low alkalinity [37].

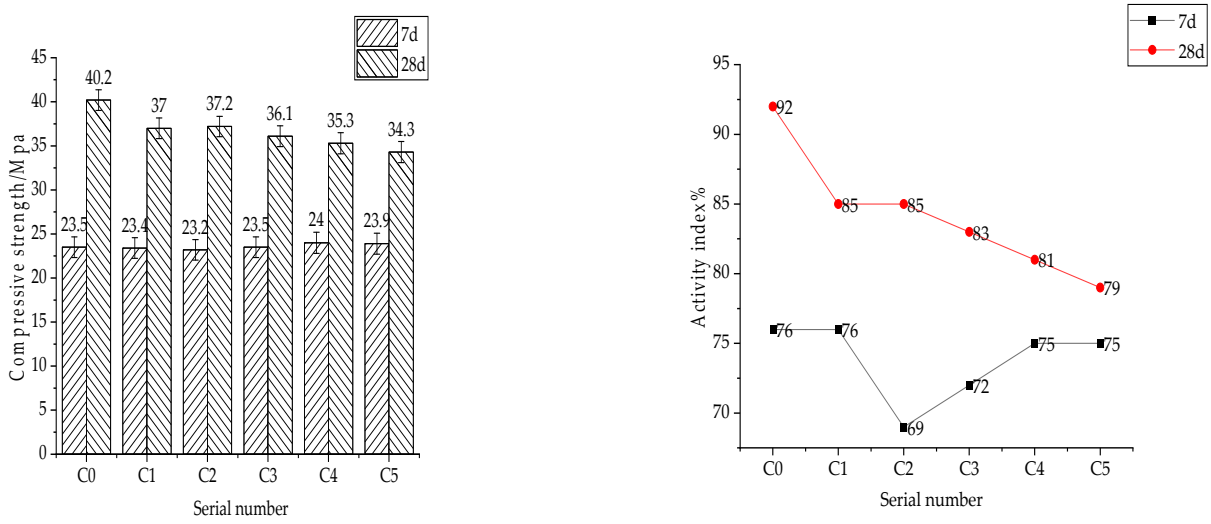

(**a**) compressive sterngth (**b**) activity index

Figure 6. Compressive strength and activity index of the ternary SCMs system in the presence of NaOH.

It can be seen from Figure 7 that the chemical activator Na_2SiO_3 to the ternary SCMs system has an inhibitory effect on the compressive strength and activity index of the whole age. For 7 d compressive strength, the change in Na_2SiO_3 content has little effect on it. At the age of 28 d, as the content of Na_2SiO_3 increased from 0% to 1.2%, the compressive strength decreased 8.8 MPa and the activity index decreased by about 20%.

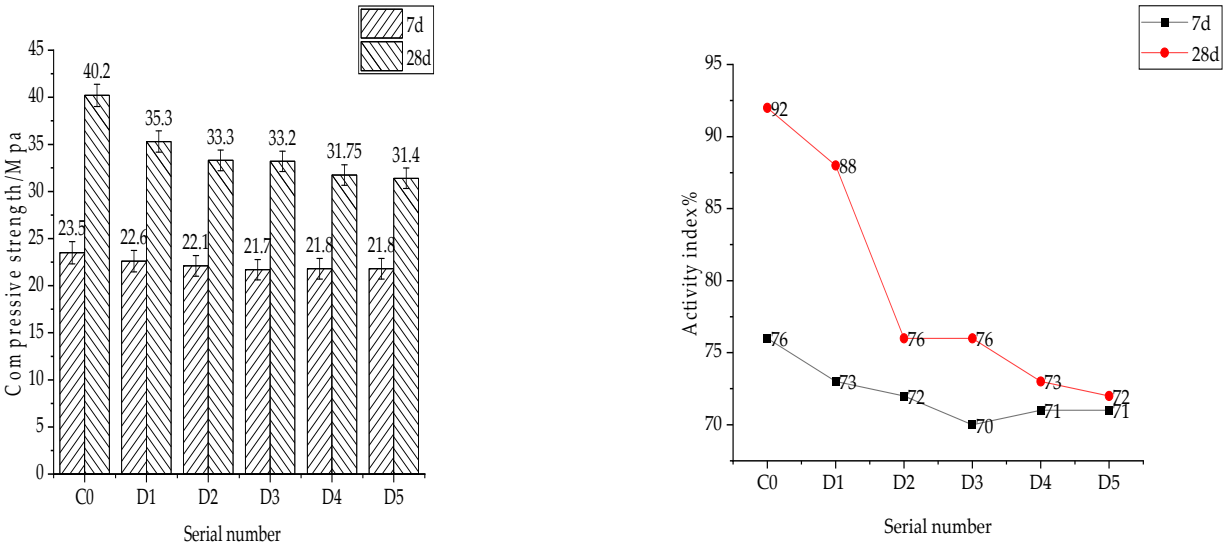

(**a**) compressive sterngth (**b**) activity index

Figure 7. Compressive strength and activity index of the ternary system in the presence of Na_2SiO_3.

When Na_2SiO_3 is dissolved in water, the following reactions occur:

$$Na_2SiO_3 + H_2O \rightarrow NaOH + H_2SiO_3 \quad (5)$$

$$Na_2SiO_3 + Ca(OH)_2 \rightarrow SiO_2 + CaSiO_3 + 2NaOH \quad (6)$$

The reasons for the inhibition of Na_2SiO_3 on the system are as follows: (a) It can be known from the Equation (6). As an accelerator, Na_2SiO_3 itself releases a large amount of

active SiO_2, so a large number of gel phases are produced at the beginning of the reaction. However, the rapidly generated gel phase covers the unreacted admixtures and prevents further dissolution [38,39]. (b) It can be seen from the Equation (5) that Na_2SiO_3 dissolves in water and consumes a certain amount of aqueous solution, so it inhibits the hydration of the whole system.

3.3. Fluidity Analysis

Figure 8 represents the variation of fluidity for different ternary SCMs systems. From the Figure 8, it can be seen that the ternary SCMs system has little change in mobility compared with the Bz group, but it reduces the fluidity to some extent. The ternary SCMs system has little effect on the fluidity by changing the proportion of materials in it.

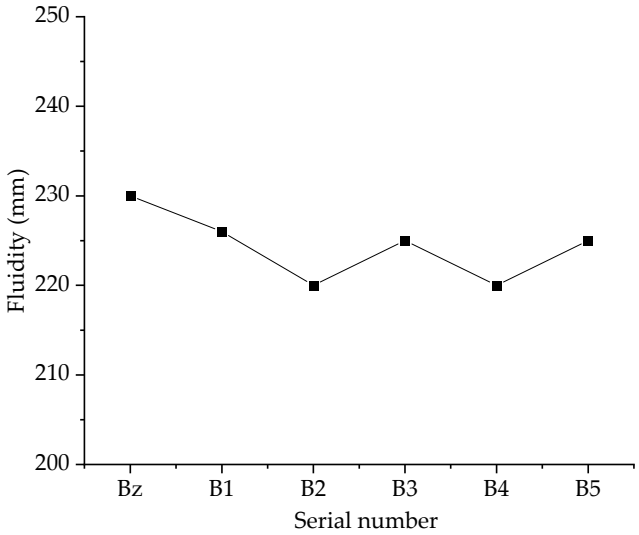

Figure 8. Fluidity Change Chart.

3.4. SEM Analysis

Figures 9–11 show the morphology of PB5, PC2, and PD2 at 28 d, respectively. Comparing Figures 9–11, we can see that there are great differences in the degree of hydration and hydration products between the two groups. As shown in Figure 9a, multiple clusters of petal-like C-S-H gels are formed in the visible range and each cluster of C-S-H gel has a larger area. In addition, the surface is flat and has fewer pores in terms of the cutting surface. Figure 9b shows that the petal-like C-S-H gel formed in the visual range has a dense structure and the overlap is tight. There are only a few flaky CH at the edge of C-S-H gel, which indicates that the degree of secondary hydration is deep [40]. CH is the weak point in the hydration product system. The higher the CH content, the lower the strength [41]. The dense C-S-H gel provides strength for the whole system. As can be seen from Figures 10a and 11a, the reaction product of the whole system is less, and the reaction degree is lower under the action of NaOH and Na_2SiO_3. It can be seen from Figures 10b and 11b that the pores of the whole system are large, the hydration products are dispersed, and the hydration products are mainly platelike CH, which indicates that the degree of secondary hydration is weak. It can be seen that the addition of NaOH has an inhibitory effect on the secondary hydration reaction, which is consistent with the compressive strengthening. It can be seen from Figure 10a that C-S-H gel is formed on the surface of unreacted IOTs, which proves that it plays a certain role in nucleation.

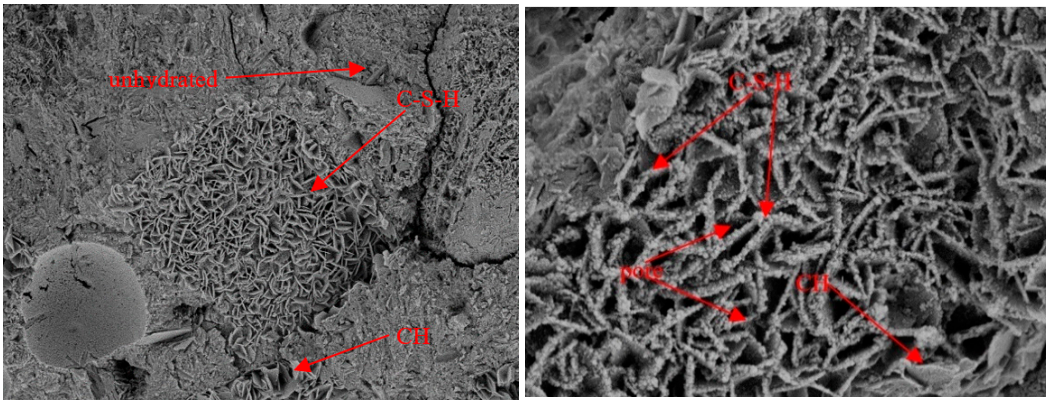

(**a**) 5000× (**b**) 20,000×

Figure 9. Hydration 28 d SEM diagram of samples with PB5.

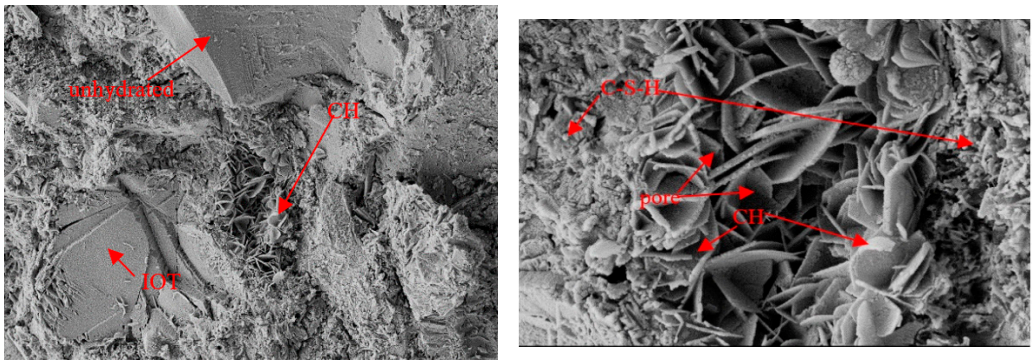

(**a**) 5000× (**b**) 20,000×

Figure 10. Hydration 28 d SEM diagram of samples with PC2.

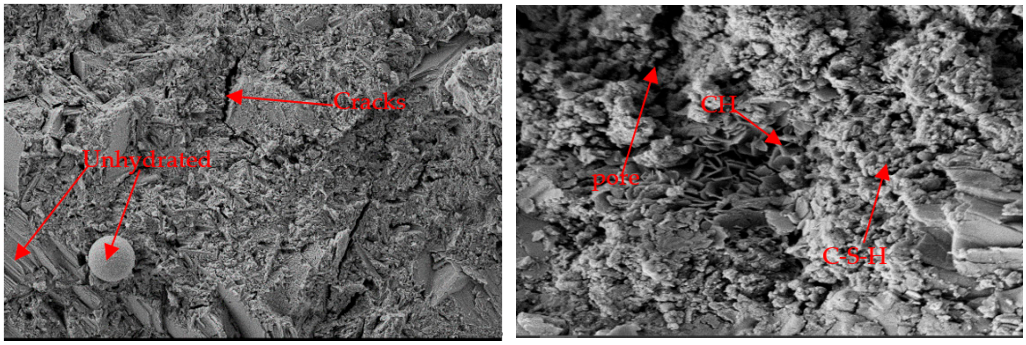

(**a**) 5000× (**b**) 20,000×

Figure 11. Hydration 28 d SEM diagram of samples with PD2.

3.5. DTA-TG Analysis

Figures 12–14 show the DTA-TG results of each experimental group at 7 days and 28 days. In each DTA-TG test, the first endothermic peak occurs between 60–120 °C. This can be attributed to dehydration of the C-S-H gel. At 400–450 °C, there is a second endothermic peak. This is caused by the dehydration of CH by heat. At 580–650 °C, there is a third endothermic peak. This is due to the decomposition of $CaCO_3$ formed by the carbonization of CH [42]. Therefore, through the TG test the content of CH can be calculated quantitatively, and the hydration degree of the system can be evaluated [39].

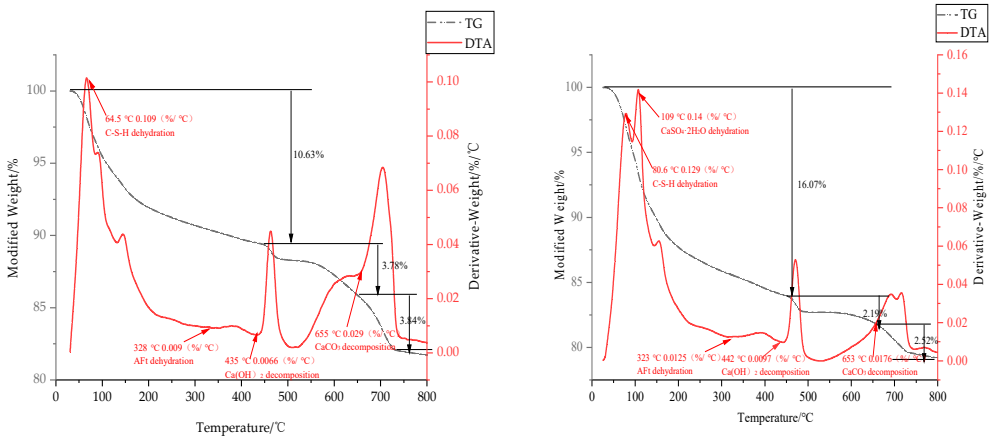

(**a**) 7 d (**b**) 28 d

Figure 12. DTA-TG curve of cement paste with PB5.

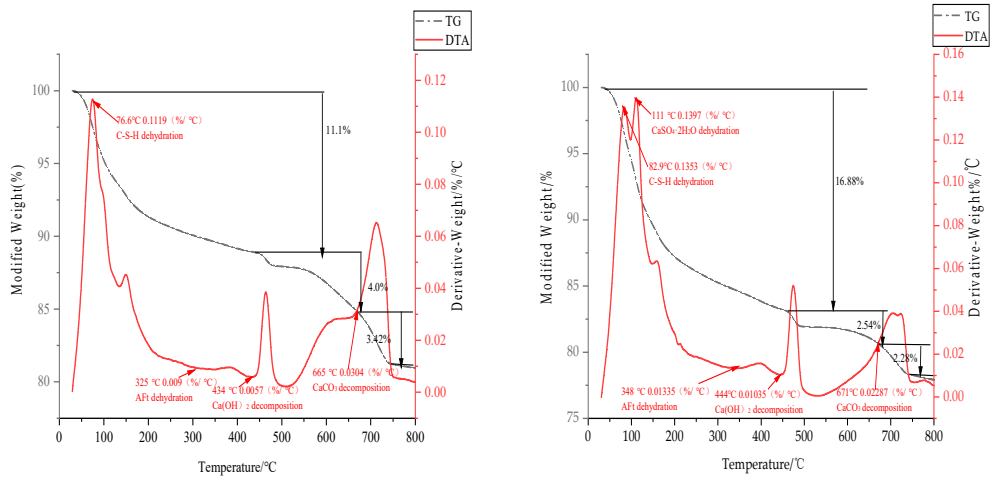

(**a**) 7 d (**b**) 28 d

Figure 13. DTA-TG curve of cement paste with PC2.

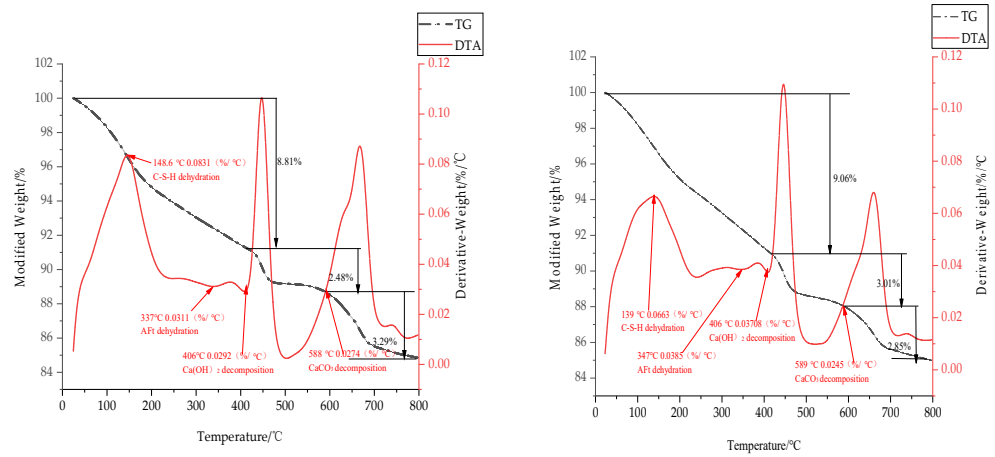

(**a**) 7 d (**b**) 28 d

Figure 14. DTA-TG curve of cement paste with PD2.

In order to directly see the hydration process of IOTs–SS–PS ternary SCMs system, the content of CH in each group of samples at different ages was calculated by the formula:

$$CH = WL_{CH} \times \frac{m_{CH}}{m_{H_2O}} + WL_{CaCO_3} \times \frac{m_{CaCO_3}}{m_{CO_2}} \quad (7)$$

In the Equation (7): CH is the relative content of calcium hydroxide in the sample (%); WL_{CH} is the mass loss of calcium hydroxide caused by the removal of water by DTA-TG; WL_{CaCO3} is the mass loss of calcium carbonate caused by the removal of water by DTA-TG; m_{CH} is the molar mass of calcium hydroxide; m_{H2O} is the molar mass of water; m_{CaCO3} is the molar mass of calcium carbonate; m_{CO2} is the molar mass of carbon dioxide.

Among them, the values of WL_{CH} and WL_{CaCO3} can be obtained by data processing of the DTA-TG curve, and the value of m_{CH} = 74 g/mol; m_{H2O} = 18 g/mol; m_{CaCO3} = 100 g/mol; and m_{CO2} = 44 g/mol. The molar mass of calcium hydroxide, water, calcium carbonate and carbon dioxide can be substituted into Equation (8).

$$CH = WL_{CH} \times \frac{74}{18} + WL_{CaCO_3} \times \frac{100}{44} \quad (8)$$

The comparison of CH content of hydration products in each sample at the hydration age of 7 d and 28 d is shown in Table 6. In the cementitious system of cement-based hardened paste, the content of CH is closely related to the degree of hydration of cement. The CH content of PB5 and PC2 decreased with the increase in hydration age. It shows that the admixture participates in the secondary hydration reaction and consumes the CH in the system [39].

Table 6. CH content in hydration products proportions.

Serial Number	Age	Dehydration Quantity of CH	Decomposition Quantity of $CaCO_3$	Quantity of CH
PB5	7 d	3.78%	3.84%	24.26%
PC2	7 d	4.00%	3.42%	24.21%
PD2	7 d	2.48%	3.29%	17.46%
PB5	28 d	2.19%	2.52%	14.73%
PC2	28 d	2.54%	2.28%	15.60%
PD2	28 d	3.01%	2.85%	18.85%

The CH content of PB5, PC2, and PD2 is different at different ages under the action of different chemical reagents, which indicates that the degree of secondary hydration reaction between composite admixture under different chemical reagents is not consistent. With the increase in age from 7 d to 28 d, the CH in the PB2 decreased by 9.53% and the CH in the PC2 decreased by 8.61%, but the CH in the PD2 increased by 1.39%. It shows that with the introduction of NaOH, Na_2SiO_3 suppresses the secondary hydration reaction, which is consistent with the compressive strengthening.

4. Conclusions

This paper studies the feasibility of a multi-SCMs system based on IOTs. SEM and DTA-TG were used to analyze the microstructure and thermal weight-loss characteristics of different gel system blocks with activator in order to determine the reason for its strength decline. This study led to the following conclusions:

- The compressive strength of the ternary SCMs system is significantly higher than that of the binary SCMs system and the unary SCMs system. Compared with the ternary SCMs system, the binary SCMs system lacking IOTs has the lowest strength, and the filling and nucleation effects of iron tailings in the ternary SCMs system cannot be ignored.
- The ternary SCMs system reached the maximum compressive strength of 40.2 MPa of the SCMs system at 28 days in the ratio of IOTs. SS:PS = 1:2:2, and the activity

index reached 92%. The difference between the 28 d compressive strength of this ternary SCMs system and that of Bz is only 3.4 Mpa, thus providing the possibility of large-scale consumption of IOTs, PS, SS.

- The nucleation of IOTs accelerates the hydration of Cao in SS and PS to produce C-S-H gel as well as $Ca(OH)_2$, while the SiO_2 in PS and IOTs reacts with the $Ca(OH)_2$ generated from SS and PS to produce C-S-H gel, and the three have a synergistic effect.
- NaOH and Na_2SiO_3 have a negative impact on the compressive strength of the system, and the hydration products of the ternary system after the addition of activator are mainly plate CH, and the hydration products are dispersed, the pores increase, and the strength decreases linearly with the increase in admixture.

Author Contributions: Y.Z. developed the initial concept of the study and secured the funding. H.S. developed the test and wrote the initial draft of the paper. X.G. and W.Z. assisted and participated in the test process. B.L. wrote the final version of the paper. All authors have read and agreed to the published version of the manuscript.

Funding: This research received no external funding.

Institutional Review Board Statement: Not applicable.

Informed Consent Statement: Not applicable.

Data Availability Statement: All data is provided in the manuscript.

Conflicts of Interest: The authors declare no conflict of interest.

References

1. Han, F.; Song, S.; Liu, J.; Huang, S. Properties of steam-cured precast concrete containing iron tailing powder. *Powder Technol.* **2019**, *345*, 292–299. [CrossRef]
2. Pacewska, B. Usage of supplementary cementitious materials: Advantages and limitations Part I. C–S–H, C–A–S–H and other products formed in different binding mixtures. *J. Therm. Anal. Calorim.* **2020**, *142*, 371–393. [CrossRef]
3. Santos, A.F.; Vaz, T.E.; Lopes, D.V.; Cardoso, O.; Quina, M.J. Beneficial use of lime mud from kraft pulp industry for drying and microbiological decontamination of sewage sludge. *J. Environ. Manag.* **2021**, *296*, 113255. [CrossRef] [PubMed]
4. Dhandapani, Y.; Santhanam, M.; Kaladharan, G.; Ramanathan, S. Towards ternary binders involving limestone additions—A review. *Cem. Concr. Res.* **2021**, *143*, 106396. [CrossRef]
5. Palankar, N.; Ravi Shankar, A.U.; Mithun, B.M. Durability studies on eco-friendly concrete mixes incorporating steel slag as coarse aggregates. *J. Clean. Prod.* **2016**, *129*, 437–448. [CrossRef]
6. Wang, W.; Liu, H. Experimental study on the mechanical properties of iron tailing sand concrete after high temperature. *Nonmet. Miner.* **2019**, *42*, 42–44. [CrossRef]
7. Fu, J.; Jones, A.M.; Bligh, M.W.; Holt, C.; Keyte, L.M.; Moghaddam, F.; Foster, S.J.; Waite, T.D. Mechanisms of enhancement in early hydration by sodium sulfate in a slag-cement blend– Insights from pore solution chemistry. *Cem. Concr. Res.* **2020**, *135*, 106110. [CrossRef]
8. Sun, H. Study on the influence of fly ash on the durability of concrete: Comment on the durability of fly ash concrete. *Concr. Cem. Prod.* **2020**, *10*, 96.
9. Han, F.; Zhou, Y.; Zhang, Z. Effect of gypsum on the properties of composite binder containing high-volume slag and iron tailing powder. *Constr. Build. Mater.* **2020**, *252*, 119023. [CrossRef]
10. Wu, R.; Liu, J. Experimental Study on the Concrete with Compound Admixture of Iron Tailings and Slag Powder under Low Cement Clinker System. *Adv. Mater. Sci. Eng.* **2018**, *2018*, 1–7. [CrossRef]
11. Liu, J.; Zhou, Y.; Wu, A. Reconstruction of broken Si–O–Si bonds in iron ore tailings (IOTs) in concrete. *Int. J. Miner. Metall. Mater.* **2019**, *26*, 1329–1336. [CrossRef]
12. Chen, Y.; Huang, F.; Li, W.; Liu, R.; Li, G.; Wei, J. Test research on the effects of mechanochemically activated iron tailings on the compressive strength of concrete. *Constr. Build. Mater.* **2016**, *118*, 164–170. [CrossRef]
13. Ma, B.-G.; Cai, L.-X.; Li, X.-G.; Jian, S.-W. Utilization of iron tailings as substitute in autoclaved aerated concrete: Physico-mechanical and microstructure of hydration products. *J. Clean. Prod.* **2016**, *127*, 162–171. [CrossRef]
14. Zhuang, S.; Wang, Q. Inhibition mechanisms of steel slag on the early-age hydration of cement. *Cem. Concr. Res.* **2021**, *140*, 106283. [CrossRef]
15. Han, X.; Feng, J.; Shao, Y.; Hong, R. Influence of a steel slag powder-ground fly ash composite supplementary cementitious material on the chloride and sulphate resistance of mass concrete. *Powder Technol.* **2020**, *370*, 176–183. [CrossRef]
16. Yang, J.; Lu, J.; Wu, Q.; Xia, M.F.; Li, X. Influence of steel slag powders on the properties of MKPC paste. *Constr. Build. Mater.* **2018**, *159*, 137–146. [CrossRef]

17. Liu, C.; Li, S.; Shen, W.; Lei, W. Comprehensive utilization of Phosphorus slag and its application in road base stabilizing cement. *World Build. Mater.* **2018**, *39*, 32–37.
18. Pang, M.; Sun, Z.; Chen, M.; Lang, J.; Dong, J.; Tian, X.; Sun, J. Influence of Phosphorus Slag on Physical and Mechanical Properties of Cement Mortars. *Materials* **2020**, *13*, 2390. [CrossRef]
19. Bezerra, C.G.; Rocha, C.A.A.; de Siqueira, I.S.; Filho, R.D.T. Feasibility of iron-rich ore tailing as supplementary cementitious material in cement pastes. *Constr. Build. Mater.* **2021**, *303*, 124496. [CrossRef]
20. Saedi, A.; Jamshidi-Zanjani, A.; Darban, A.K. A review on different methods of activating tailings to improve their cementitious property as cemented paste and reusability. *J. Environ. Manag.* **2020**, *270*, 110881. [CrossRef]
21. Sun, J.; Zhang, Z.; Zhuang, S.; He, W. Hydration properties and microstructure characteristics of alkali–activated steel slag. *Constr. Build. Mater.* **2020**, *241*, 118141. [CrossRef]
22. Xie, F.; Liu, Z.; Zhang, D.; Wang, J.; Wang, D.; Ni, J. The effect of NaOH content on rheological properties, microstructures and interfacial characteristic of alkali activated phosphorus slag fresh pastes. *Constr. Build. Mater.* **2020**, *252*, 119132. [CrossRef]
23. *GB175-2007*; Common Portland Cement. China Quality and Standards Publishing & Media Co., Ltd.: Beijing, China, 2007.
24. *GB/T51003-2014*; Technical Code for Application of Mineral Admixture. China Quality and Standards Publishing & Media Co., Ltd.: Beijing, China, 2014.
25. *GB/T 17671-1999*; Method of Testing Cements—Determination of Strength. China Quality and Standards Publishing & Media Co., Ltd.: Beijing, China, 1999.
26. *GB/T12957-2005*; Test Method for Activity of Industrial Waste Slag Used as Addition to Cement. China Quality and Standards Publishing & Media Co., Ltd.: Beijing, China, 2005.
27. *GB/T2419-2005*; Test Method for Fluidity of Cement Mortar. China Quality and Standards Publishing & Media Co., Ltd.: Beijing, China, 2005.
28. Ming, Z.; Qianming, M.; Rongxin, G.; Pang, W. Mechanical Properties of Phosphorus Slag-Portland Cement Composite and Alkali Phosphorus Slag Cementitious Materials. *Bull. Chin. Ceram. Soc.* **2020**, *39*, 376–382.
29. Yu, L.; Wang, Q.; Wu, K.; Tan, Z.; Pan, F.; Yang, Z.; De Schutter, G. Identification of multi-scale homogeneity of blended cement concrete: Macro performance, micro and meso structure. *J. Therm. Anal.* **2022**, 1–12. [CrossRef]
30. Lothenbach, B.; Scrivener, K.; Hooton, R.D. Supplementary cementitious materials. *Cem. Concr. Res.* **2011**, *41*, 1244–1256. [CrossRef]
31. Martins, A.C.P.; Franco de Carvalho, J.M.; Costa, L.C.B.; Andrade, H.D.; Varela de Melo, T.; Ribeiro, J.C.L.; Pedroti, L.G.; Peixoto, R.A.F. Steel slags in cement-based composites: An ultimate review on characterization, applications and performance. *Constr. Build. Mater.* **2021**, *291*, 123265. [CrossRef]
32. Wang, D.; Shi, C.; Farzadnia, N.; Shi, Z.; Jia, H. A review on effects of limestone powder on the properties of concrete. *Constr. Build. Mater.* **2018**, *192*, 153–166. [CrossRef]
33. Li, C.; Sun, H.; Yi, Z.; Li, L. Innovative methodology for comprehensive utilization of iron ore tailings: Part 2: The residues after iron recovery from iron ore tailings to prepare cementitious material. *J. Hazard. Mater.* **2010**, *174*, 78–83. [CrossRef]
34. Hasannejad, M.; Berenjian, J.; Pouraminian, M.; Larijani, A.S. Studying of microstructure, interface transition zone and ultrasonic wave velocity of high strength concrete by different aggregates. *J. Build. Pathol. Rehabil.* **2021**, *7*, 1–15. [CrossRef]
35. Wang, Y.; Shi, C.; Ma, Y.; Xiao, Y.; Liu, Y. Accelerators for shotcrete–Chemical composition and their effects on hydration, microstructure and properties of cement-based materials. *Constr. Build. Mater.* **2021**, *281*, 122557. [CrossRef]
36. You, J.; Yoo, J.-S.; Kum, K.-Y.; Hong, S.-H. Hydration behavior and radiopacity of strontium substituted Ca3SiO5 cement. *J. Korean Ceram. Soc.* **2021**, *58*, 330–336. [CrossRef]
37. Huang, W.; Kazemi-Kamyab, H.; Sun, W.; Scrivener, K. Effect of replacement of silica fume with calcined clay on the hydration and microstructural development of eco-UHPFRC. *Mater. Des.* **2017**, *121*, 36–46. [CrossRef]
38. Du, J.; Meng, W.; Khayat, K.H.; Bao, Y.; Guo, P.; Lyu, Z.; Abu-obeidah, A.; Nassif, H.; Wang, H. New development of ultra-high-performance concrete (UHPC). *Compos. Part B Eng.* **2021**, *224*, 109220. [CrossRef]
39. He, Y.; Liu, S.; Zhang, X.; Liu, W.; Liao, G.; Xu, M. Influence of triethanolamine on mechanical strength and hydration performance of blended cement containing fly ash, limestone and slag. *J. Build. Eng.* **2021**, *44*, 102879. [CrossRef]
40. Wang, Y. *Evaluation of Volcanic Ash Activity of Lithium Slag and Its Microstructural Properties of Composite Cementitious Materials*; China University of Mining and Technology: Beijing, China, 2018.
41. Lu, X.; Wang, S.; Ye, Z.; Li, C.; Cheng, X. Study on the hydration product of ettringite in cement paste with ethanol-diisopropanolamine. *J. Therm. Anal. Calorim.* **2020**, *139*, 1007–1016. [CrossRef]
42. Piao, C.A. *The Activation Process and Mechanism of Iron Tailings Powder and Its Influence on Concrete Performance*; China University of Mining and Technology: Beijing, China, 2017.